

Simplified Mesoscale Lattice Boltzmann Numerical Model for Prediction of Natural Convection in a Square Enclosure filled with Homogeneous Porous Media

C.S.NOR AZWADI

Faculty of Mechanical Engineering
Universiti Teknologi Malaysia
81310 Skudai Johor
MALAYSIA

azwadi@fkm.utm.my <http://www.fkm.utm.my/~azwadi/>

M.A.M. IRWAN

Faculty of Mechanical Engineering
Universiti Teknikal Malaysia Melaka
76109 Durian Tunggal Melaka
MALAYSIA

mohdirwan@utem.edu.my

Abstract: - The lattice Boltzmann method (LBM) is applied to a generalised isotropic porous media model in a square geometry by introducing a force term to the evolution equation and a porosity to the density equilibrium distribution function. The temperature field is obtained by simulating a simplified thermal model which uses less velocity directions for the equilibrium distribution function and neglects the compression work done by the pressure and the viscous heat dissipation. The reliability of this model for natural convective heat transfer simulation is studied by comparing with results from previous simulations at a porosity value, $\varepsilon = 0.9999$. The model is then used for simulation at $\varepsilon = 0.4, 0.6$ and 0.9 at three different Rayleigh numbers. Comparison of solutions with previous works confirms the applicability of the present approach.

Key-Words: - lattice Boltzmann method, distribution function, Boussinesq approximation, porous media, convective heat transfer,

1 Introduction

Flow in an enclosure driven by buoyancy force is a fundamental problem in fluid mechanics. This type of flow can be found in certain engineering applications within electronic cooling technologies, in everyday situation such as roof ventilation or in academic research where it may be used as a benchmark problem for testing newly developed numerical methods. A classic example is the case where the flow is induced by differentially heated walls of the cavity boundaries. Two vertical walls with constant hot and cold temperature is the most well defined geometry and was studied extensively in the literature. A comprehensive review was presented by Davis[1]. The analysis of flows and heat transfer in a differentially heated side walls was extended to the inclusion of porous media in the system. Darcy's equation was earlier used by the researchers to study the natural convection phenomenon in porous media. However, previous results indicated that the equation was only applicable at low flow velocity condition[2]. For higher flow velocity, modifications to the original equation are required which need to consider the non-linear drag due to the solid matrix[3] and viscous stresses by the solid boundary[4]. These two factors may not affect the study in low velocity but

it must be considered for high velocity studies. The combination of these two equations is known as Brinkman-Forchheimer equation. The behaviour of this non-Darcian condition was shown in physical experiment by Prasad et al[5]. However, due to lack of generality in the model for the prediction at medium with variable porosity, a generalised model was then developed in 1997 by Nithiarasu et al[6].

Since the introduction to the lattice Boltzmann method (LBM)[7][8][9][10], a mesoscale numerical scheme based on particle distribution function, LBM has developed to be as an alternative numerical tool in solving wide range of fluid flow problem. LBM has been proven to be a better tool to predict isothermal and thermal fluid flow[11][12][13], magnetohydrodynamics[14], turbulent fluid flow[15], multiphase fluid flow[16][17][18], flow in microchannel[19][20], etc.

Historically, LBM was derived from lattice gas (LG) automata[21]. It utilizes particle distribution function to describe collective behaviors of fluid molecules. The macroscopic quantities such as density, velocity and temperature are then obtained through moment integrations of distribution function. In comparison with other numerical schemes, LBM is a bottom up approach, derives the Navier-Stokes equation from statistical behavior of particles dynamics. The imaginary propagation and

collision processes of fluid particles are reconstructed in the formulation of LBM scheme. These processes are represented by the evolution of particle distribution function $f(x, t)$, which describes the statistical population of particles at location x and time t . The advantages of LBM include simple calculation procedure [22], suitability for parallel computation [23], ease and robust handling of multiphase flow [24], complex geometries [25], interfacial dynamics and others [26][27]. A few standard benchmark problems have been simulated by LBM and the results are found to agree well with the corresponding Navier-Stokes solutions[28][29].

Our literature study found that there are several investigations have been conducted using the LBM to understand the thermal fluid flow in an enclosure[8][9][12]. However, most of them applied the same lattice model to predict the evolution of velocity and temperature fields in the system. Combination of nine-lattice model for the density and also the same model for the temperature distribution functions is the most common approach by the previous researchers. Currently, one of present authors has developed the simplest lattice model to predict the evolution of temperature field[11]. Unfortunately, the developed model was found not in good agreement with the literature studies when predicting athermal flow at high Rayleigh numbers. This was due to the limitation of the model where unable to capture high speed of fluid flow in the system[11]. The presence of the porous medium is believed to decelerate the flow although depended on the magnitude of the porosity. Therefore, the objective of present paper is to reconsider the newly developed model and predict the fluid and thermal flow in an enclosure filled with porous medium at high Rayleigh numbers.

The current study is summarized as follow: two-dimensional fluid flow and heat transfer in a porous medium filled in square cavity is investigated numerically. The two sidewalls are maintained at different temperatures while the top and bottom walls are set as an adiabatic wall. Here, we fix the aspect ratio to unity. The flow structures and heat transfer mechanism are highly dependent upon the porosity of the medium. By also adopting the Rayleigh number as a continuation parameter, the flow structure and heat flow represented by the streamlines and isotherms lines can be identified as a function of porosity. Comparisons of results among those published in literature are carried out in terms of a computed averaged Nusselt number. Section two of this paper presents the governing equations for the case study in hand and introduces the numerical method which will be adopted for its

solution. Meanwhile section three presents the computed results and provide a detailed discussion. The final section of this paper concludes the current study.

2 Thermal Lattice Boltzmann Method

We start from the derivation of the internal energy density distribution from the continuous Boltzmann equation. The Boltzmann equation with the Bhatnagar-Gross-Krook (BGK), or single-relaxation-time approximation[30][31]with external force is given by

$$\frac{\partial f}{\partial t} + \mathbf{c} \frac{\partial f}{\partial \mathbf{x}} = -\frac{1}{\tau_f} (f - f^{eq}) + F_i \quad (1)$$

where $f = f(\mathbf{x}, \mathbf{c}, t)$ is the single-particle distribution function, \mathbf{c} is the microscopic velocity, τ_f is the relaxation time due to collision, F_i is the external force, and f^{eq} is the local Maxwell-Boltzmann equilibrium distribution function given by

$$f^{eq} = \rho \left(\frac{1}{2\pi RT} \right)^{D/2} \exp \left\{ -\frac{(\mathbf{c} - \mathbf{u})^2}{2RT} \right\} \quad (2)$$

where R is the ideal gas constant, D is the dimension of the space, and ρ , u , and T are the macroscopic density of mass, velocity, and temperature respectively. The macroscopic variables ρ , u , and T can be evaluated as the moment to the distribution function

$$\rho = \int f d\mathbf{c}, \rho \mathbf{u} = \int \mathbf{c} f d\mathbf{c}, \frac{\rho D R T}{2} = \int \frac{(\mathbf{c} - \mathbf{u})^2}{2} f d\mathbf{c} \quad (3)$$

By applying the Chapman-Enskog expansion[30], the above equations can lead to macroscopic continuity, momentum and energy equation. However the Prandtl number obtained is fixed to a constant value[11]. This is caused by the use of single relaxation time in the collision process. The relaxation time of energy carried by the particles to its equilibrium is different to that of momentum. Therefore we need to use a different two relaxation times to characterize the momentum and energy transport. This is equivalent in introducing a new distribution function to define energy.

To obtain the new distribution function modeling energy transport, the new variable, the

internal energy density distribution function is introduced

$$g = \frac{(\mathbf{c} - \mathbf{u})^2}{DR} f \quad (4)$$

Substituting Eq. (4) into Eq. (1) results in

$$\frac{\partial g}{\partial t} + \mathbf{c} \frac{\partial g}{\partial \mathbf{x}} = -\frac{1}{\tau_g} (g - g^{eq}) + F_g + fq \quad (5)$$

where

$$g^{eq} = \frac{(\mathbf{c} - \mathbf{u})^2}{DR} f^{eq} \quad (6)$$

$$F_g = \frac{(\mathbf{c} - \mathbf{u})^2}{2} F_f \quad (7)$$

and

$$q = \frac{\mathbf{c} - \mathbf{u}}{2} \left(\frac{\partial \mathbf{u}}{\partial t} + \mathbf{c} \cdot \nabla \mathbf{u} \right) \quad (8)$$

are the equilibrium distribution function for internal energy, the term due to the external force, and the heat dissipation term respectively. Equation (4) represents the internal energy carried by the particles and therefore Eq. (5) can be called as the evolution equation of internal energy density distribution function. The macroscopic variables can thus be redefined in term of distribution functions f and g as

$$\rho = \int f d\mathbf{c}, \rho \mathbf{u} = \int \mathbf{c} f d\mathbf{c}, \rho T = \int g d\mathbf{c} \quad (9)$$

In this paper, we will apply the method proposed by Azwadi and Tanahashi[11] which consider that the viscous heat dissipation can be neglected for the incompressible flow. So here, we neglect the dissipation and the external force in the evolution equation of internal energy density distribution function as follow

$$\frac{\partial g}{\partial t} + \mathbf{c} \frac{\partial g}{\partial \mathbf{x}} = -\frac{1}{\tau_g} (g - g^{eq}) \quad (10)$$

By omitting the dissipation term, the complicated gradient operator in the evolution equation of internal energy distribution function can be dropped.

In order to apply the lattice Boltzmann scheme

into the digital computer, the evolution equation of the continuous lattice Boltzmann BGK equation for the momentum and energy needs to be discretised in the velocity space. Expanding both of the equilibrium distribution function up to \mathbf{u}^2 and applying some mathematics manipulations results in[32]

$$f^{eq} = \rho \left(\frac{1}{2\pi RT} \right)^{D/2} \exp \left\{ -\frac{\mathbf{c}^2}{2RT} \right\} \left[1 + \frac{\mathbf{c} \cdot \mathbf{u}}{RT} + \frac{(\mathbf{c} \cdot \mathbf{u})^2}{2(RT)^2} - \frac{\mathbf{u}^2}{2RT} \right] \quad (11)$$

$$g^{eq} = \rho T \left(\frac{1}{2\pi RT} \right)^{D/2} \exp \left\{ -\frac{\mathbf{c}^2}{2RT} \right\} \left[1 + \frac{\mathbf{c} \cdot \mathbf{u}}{RT} \right] \quad (12)$$

To recover the macroscopic equation, the zeroth-to third-order moments of f^{eq} and zeroth-to second-order moments of g^{eq} must be exact. In general

$$I_f = \int \mathbf{c}^m f^{eq} d\mathbf{c}, I_g = \int \mathbf{c}^m g^{eq} d\mathbf{c} \quad (13)$$

where I_f and I_g should be exact for m equal to zero till three and zero till two respectively. Equation (13) can be calculated by using the Gauss-Hermite quadrature. Hence, the Gauss-Hermite quadrature must consistently give accurate result for quadratures of zeroth-to-fifth-order of velocity moment of f^{eq} and zeroth-to-third order for g^{eq} . This implies that we can choose third-order Gauss-Hermite quadrature in evaluating I_f and second order Gauss-Hermite quadrature for I_g . As a result, we obtained the expression for the discretised density equilibrium distribution function as follows

$$f_i^{eq} = \rho \omega_i \left[1 + 3\mathbf{c} \cdot \mathbf{u} + 4.5(\mathbf{c} \cdot \mathbf{u})^2 - 1.5\mathbf{u}^2 \right] \quad (14)$$

where the weights are $\omega_1 = 4/9$, $\omega_2 = \omega_3 = \omega_4 = \omega_5 = 1/9$ and $\omega_6 = \omega_7 = \omega_8 = \omega_9 = 1/36$. This is equivalent to the well-known D2Q9 model. Lattice structure of this model is shown in Fig. 1.

After some modifications in order to satisfy macroscopic energy equation via Chapman-Enskog expansion procedure, the discretised internal energy density distribution function is obtained as

$$g_{1,2,3,4}^{eq} = \frac{1}{4} \rho T [1 + \mathbf{c} \cdot \mathbf{u}] \quad (15)$$

This new type of lattice structure for internal energy density distribution is shown in Fig. 2.

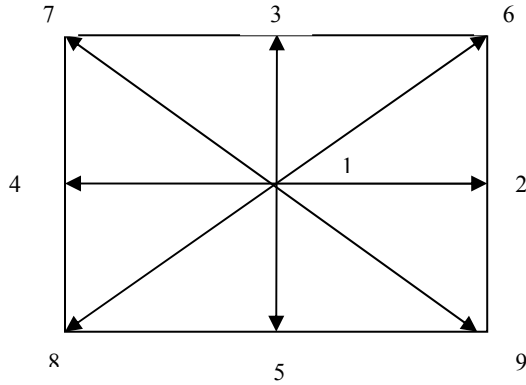


Fig. 1. Lattice structure for density distribution function.

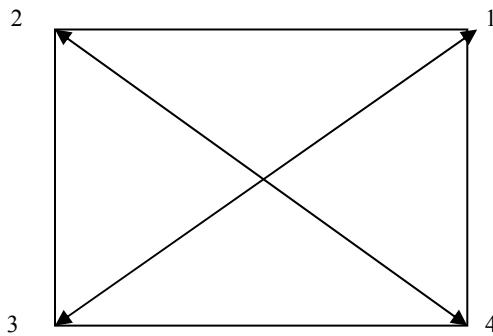


Fig. 2. Lattice structure for internal energy density distribution function.

Through a multiscaling expansion, the mass and momentum equations can be derived for D2Q9 model. The detail derivation of this is given by He and Luo et al[13] and will not be shown here. The kinematic viscosity is given by

$$\nu = \frac{2\tau_f - 1}{6} \quad (16)$$

The energy equation at the macroscopic level can be expressed as follows

$$\frac{\partial}{\partial t} \rho T + \nabla \cdot \rho \mathbf{u} T = \chi \nabla^2 (\rho T) \quad (17)$$

where χ is the thermal diffusivity. Thermal

diffusivity and the relaxation time of internal energy distribution function is related as

$$\chi = \tau_g - \frac{1}{2} \quad (18)$$

3 Numerical Simulations

The physical domain of the problem is represented in Fig. 3.

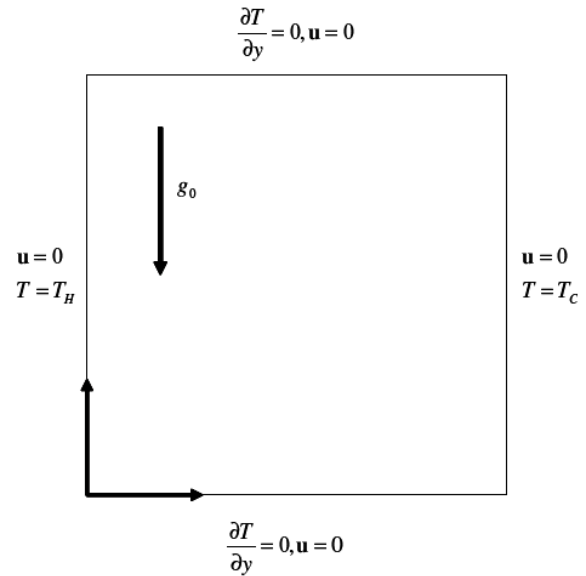


Fig. 3: Physical domain of problem

The system consists of a square enclosure with sides of length L and differentially heated hot left and cold right walls. The temperature difference between the left and right walls introduces a temperature gradient in a fluid, and the consequent density difference induces a fluid motion, that is, convection.

There are two dimensionless parameters which govern the characteristic of thermal and fluid flow in the enclosure; the Prandtl and Rayleigh numbers defined as follow

$$Pr = \frac{\nu}{\chi} \quad (18)$$

$$Ra = \frac{g\beta(T_H - T_C)L^3}{\nu\chi}$$

The Boussinesq approximation is applied to the buoyancy force term. With this approximation, it is assumed that all the fluid properties are constant except for density change with temperature.

$$\mathbf{G} = \beta g(T - T_m)\mathbf{j} \quad (19)$$

where β is the thermal expansion coefficient, g is the acceleration due to gravity, T_m is the average temperature and \mathbf{j} is the vertical direction opposite to that of gravity.

In order to simulate the fluid flow and heat transfer in a porous medium, we need to consider the Brinkman-Forchheimer equation as a governing equation as follow

$$\frac{\partial \mathbf{u}}{\partial t} + (\mathbf{u} \cdot \nabla) \left(\frac{\mathbf{u}}{\varepsilon} \right) = -\frac{1}{\rho} \nabla(\varepsilon p) + \nu_e \nabla^2 \mathbf{u} + \mathbf{F} \quad (20)$$

where ε is the porosity of the medium, ν_e the effective viscosity. To correctly reproduce the hydrodynamics of fluid in porous medium, the body force \mathbf{F} must include the viscous diffusion and inertia effects as follow

$$\mathbf{F} = -\frac{\varepsilon \nu}{K} \mathbf{u} - \frac{1.75}{\sqrt{150 \varepsilon K}} |\mathbf{u}| \mathbf{u} + \varepsilon \mathbf{G} \quad (21)$$

where ν is the kinematic viscosity and K is the permeability and defined as

$$K = Da \times H \quad (22)$$

where Da is the Darcy number and H is the characteristic length.

Recently, Seta et al[33] has proved that the force term to be incorporated in the LBM scheme must be written as follow

$$F_i = \omega_i \rho \left[1 - \frac{1}{2\tau_f} \right] \left[3\mathbf{c}_i \cdot \mathbf{F} + \frac{9(\mathbf{u}\mathbf{F} : \mathbf{c}_i \mathbf{c}_i)}{\varepsilon} - \frac{3\mathbf{u} \cdot \mathbf{F}}{\varepsilon} \right] \quad (23)$$

This force term is used to account for porosity effects while neglecting the compression work done by the pressure and the viscous heat dissipation. The porosity effects include non-linear drag due to the solid matrix and viscous stresses by the solid boundary. Therefore the fluid velocity must be redefined as

$$\mathbf{u} = \frac{\mathbf{v}}{\mathbf{c}_0 + \sqrt{\mathbf{c}_0^2 + \mathbf{c}_1 |\mathbf{v}|}} \quad (24)$$

where

$$\mathbf{v} = \frac{\sum \mathbf{c}_i f_i}{\rho} + \frac{\Delta t}{2} \varepsilon \mathbf{G} \quad (25)$$

$$c_0 = \frac{1}{2} \left(1 + \varepsilon \frac{\Delta t \nu}{2K} \right) \quad (26)$$

and

$$c_1 = \varepsilon \frac{\Delta t}{2} \frac{1.75}{\sqrt{150 \varepsilon^3 K}} \quad (27)$$

3.1 Simulation Results

Before we carry out computational for the flow and heat transfer inside the porous medium, we firstly validate our code by computing the convective heat transfer phenomenon without the presence of porous medium. Vast numerical and experimental results can be easily obtained from the literature for the sake of comparison with our predicted results. To simulate the fluid flow and heat transfer using the newly developed computational code, we set up the value of porosity approaches to unity and very high Darcy number. This is to ensure very minimum effect of porosity in the Brinkman-Forchheimer equation and thus creates a condition similar to the original Navier Stokes equation for free fluid flows.

In Table 1, the average Nusselt number obtained for this condition are compared with results from similar simulation condition by using finite element method[6], LBM proposed by Seta et al[33] and Conventional Navier-Stokes solution published by Davis [1]. As can be seen form the Table, the computed Nusselt numbers agree well with the other studies.

Table 1 Comparison of the present results with single phase fluid flow ($\varepsilon = 0.9999$).

Ra	Average Nusselt Number			
	Ref[6]	Ref[33]	Ref[1]	Present
10^3	1.127	1.117	1.116	1.117
10^4	2.245	2.244	2.238	2.244

The plots of streamline and isotherm lines are shown in Figs. 4 and 5. As can be seen from the figures, at $Ra = 10^3$, streamlines are those of a single vortex, with its centre in the centre of the system. The corresponding isotherms are parallel to the heated walls, indicating that the most heat transfer mechanism is by conduction. As the Rayleigh number increase, ($Ra = 10^4$), the central streamline is distorted into an elliptic shape and the effects of

convection can be seen in the isotherms. The velocity components for $Ra = 10^3$ and $Ra = 10^4$ are shown in Fig. 6 and Fig. 7. It can be seen from these figures that as the Rayleigh number increases, the velocity maximum moves closer to the wall and its amplitude increases. All of the plotted figures are in good comparisons with the readily published data in literature[8][9][11].

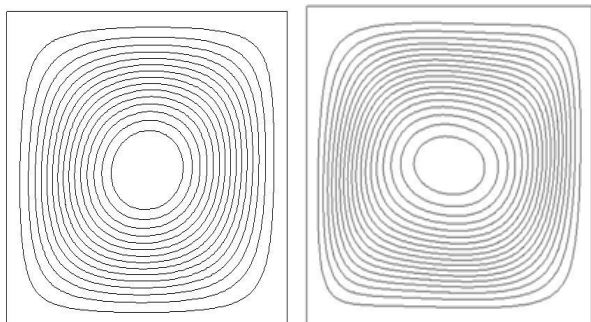


Fig. 4: Streamline plots for $Ra = 10^3$ (left) and 10^4 (right)

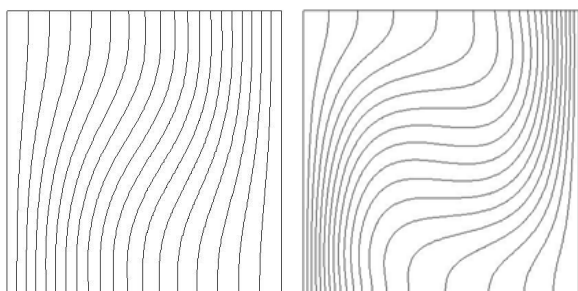


Fig. 5: Isotherms plots for $Ra = 10^3$ (left) and 10^4 (right)

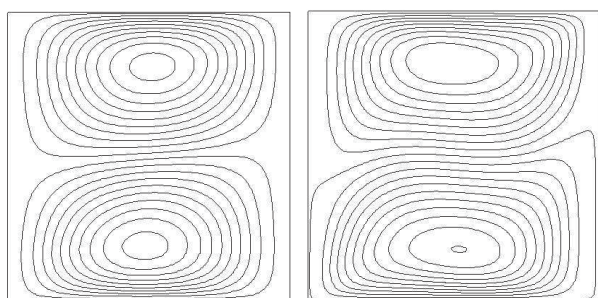


Fig. 6: Plots of horizontal velocity components for $Ra = 10^3$ (left) and 10^4 (right) plot

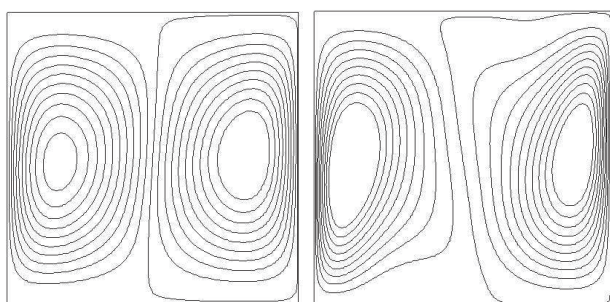


Fig. 7: Plots of vertical velocity components for $Ra = 10^3$ (left) and 10^4 (right) plot

The applicability of the present model is verified with other works by considering similar Brinkman-Forcheimer model for $p_r = 1.0$ and $\epsilon = 0.4, 0.6$ and 0.9 . In Tabs. 2 to 4, the average Nusselt number calculated by the present model is compared with results from similar simulation condition by using FEM by Nithiarasu et.al. [6] and LBM Brinkman-Forcheimer equation using D2Q9 for thermal equilibrium distribution function by Seta et. al [33].

Table 2 Comparison of the present results with the Brinkman-Forcheimer model for $\epsilon = 0.4$

Da	Ra	Average Nusselt Number		
		Ref[6]	Ref[33]	Present
10^{-2}	10^3	1.010	1.007	1.008
	10^4	1.408	1.362	1.313
	10^5	2.983	2.992	2.982

Table 3 Comparison of the present results with the Brinkman-Forcheimer model for $\epsilon = 0.6$

Da	Ra	Average Nusselt Number		
		Ref[6]	Ref[33]	Present
10^{-2}	10^3	1.015	1.012	1.012
	10^4	1.530	1.493	1.495
	10^5	2.983	2.992	2.982

Table 4 Comparison of the present results with the Brinkman-Forcheimer model for $\epsilon = 0.9$

Da	Ra	Average Nusselt Number		
		Ref[6]	Ref[33]	Present
10^{-2}	10^3	1.023	1.017	1.019
	10^4	1.64	1.633	1.721
	10^5	3.91	3.902	3.635

As can be seen from the table, at the simulation of Rayleigh number 10^3 and 10^4 , the obtained Nusselt numbers agree well with the other previous works. The predicted results feature similar to the non-Darcian behavior obtained by experimental investigation reported by Prasad et al [5]:

- 1) for a given Darcy number and porosity, the Nusselt number increases with Rayleigh number
- 2) for a given Rayleigh number and porosity, the Nusselt number increases with Darcy number due to the high permeability of the medium which accelerates flow velocities
- 3) for low Darcy and Rayleigh numbers, the Nusselt number is not influenced by the value of Darcy, Rayleigh numbers and porosity.

- 4) for a given Rayleigh and Darcy number, the Nusselt number approximately linearly increases with porosity.

However, for Rayleigh number of 10^5 the result deviates from the other previous results due to higher spatial resolution requirement. In order to produce an acceptable result, a mesh size of at least 401×401 is required [11].

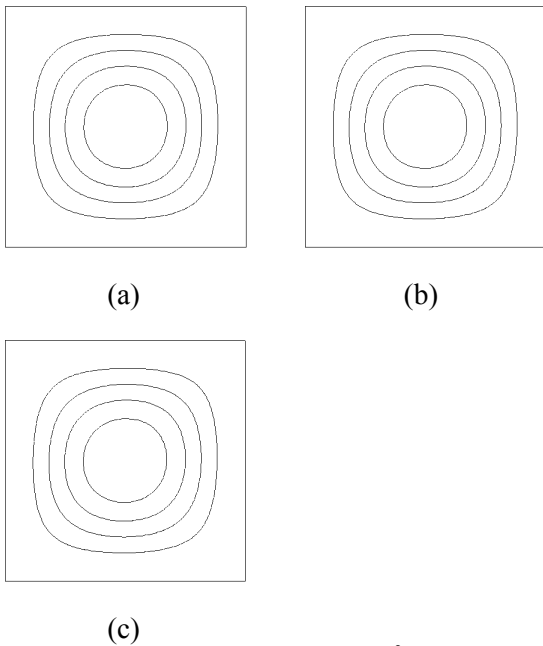


Fig. 8: Streamline plots for $Ra = 10^3$ and (a) $\epsilon = 0.4$, (b) $\epsilon = 0.6$ (c) $\epsilon = 0.9$

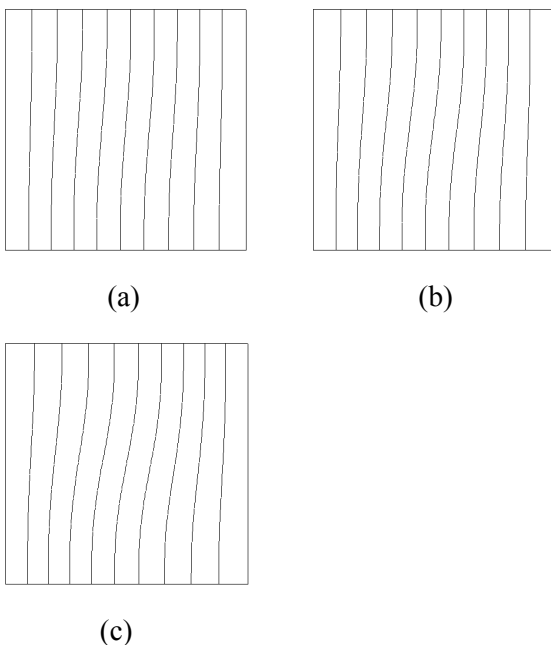


Fig. 9: Isotherms plots for $Ra = 10^3$ and (a) $\epsilon = 0.4$, (b) $\epsilon = 0.6$ (c) $\epsilon = 0.9$

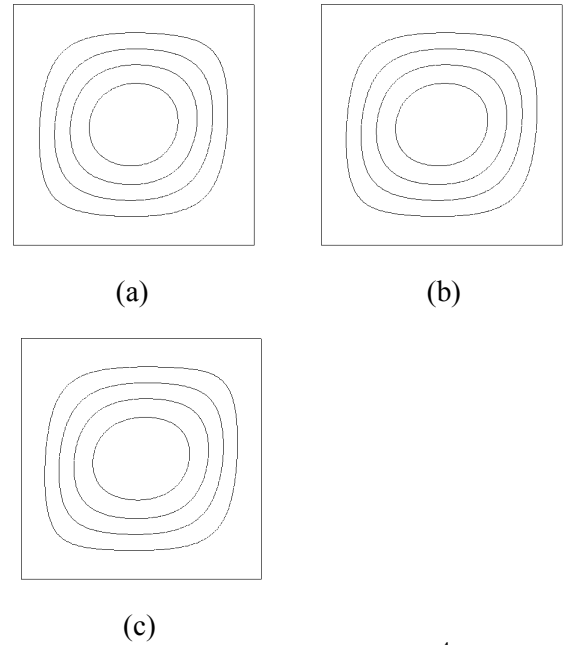


Fig. 10: Streamline plots for $Ra = 10^4$ and (a) $\epsilon = 0.4$, (b) $\epsilon = 0.6$ (c) $\epsilon = 0.9$

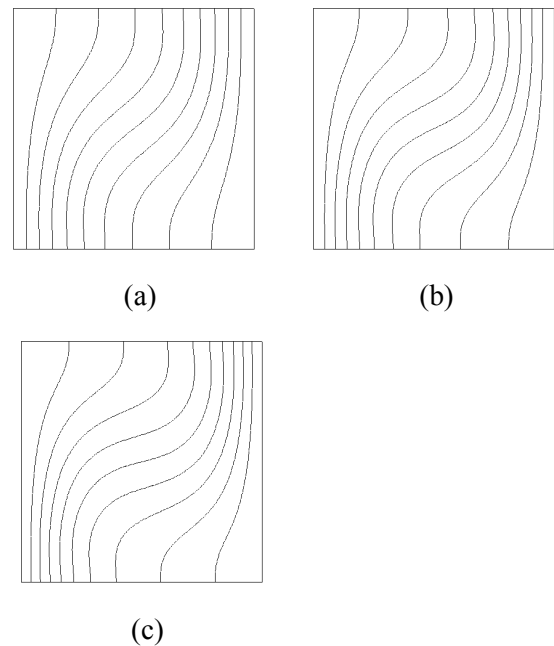


Fig. 11: Isotherms plots for $Ra = 10^4$ and (a) $\epsilon = 0.4$, (b) $\epsilon = 0.6$ (c) $\epsilon = 0.9$

Plots of the computed streamlines and isotherms line for three different values of porosity at three different values of Rayleigh numbers are shown in Figs. 8-11. At $Ra = 10^3$, the streamlines form a clockwise flow pattern and the main vortex exists with its center at the center of the system. At this value of Rayleigh number, the porosity does not seem to significantly affect the flow patterns, as

there are no changes on the streamline pattern for different value of porosity is observed. However, as the porosity increase, there is a relatively small tendency of the lines to become less parallel to the differentially heated walls. This is due to the fact that the inertial and non-linear drag terms are becoming less significant and leads to higher flow velocity in the system.

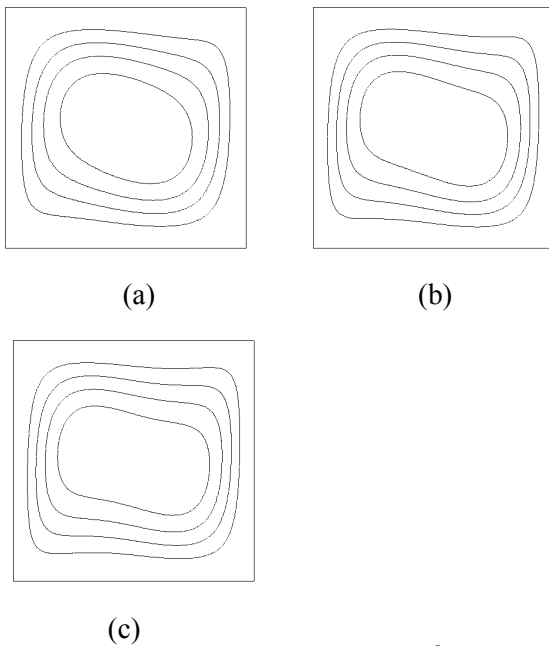


Fig. 12: Streamline plots for $Ra = 10^5$ and (a) $\varepsilon = 0.4$, (b) $\varepsilon = 0.6$ (c) $\varepsilon = 0.9$

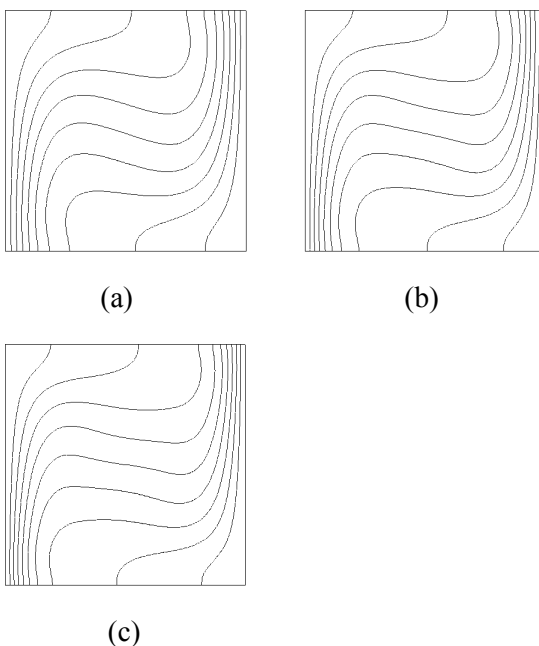


Fig. 13: Isotherms plots for $Ra = 10^5$ and (a) $\varepsilon = 0.4$, (b) $\varepsilon = 0.6$ (c) $\varepsilon = 0.9$

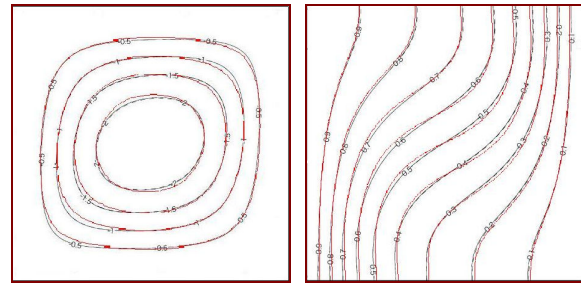


Fig. 14: Comparison of streamlines and isotherms between Navier-Stokes solution and current approach

For the simulation at $Ra = 10^4$, we can see from the streamline plots that the vortex is transformed into an elliptic shape. As the porosity increases, the shape becomes more and more elliptic shape due to higher velocity drags the outer vortex. The isotherms lines become parallel to the top and bottom walls at the center region of the enclosure indicates that the convection type dominates the heat transfer mechanism near this area. However, near the differentially heated walls, the viscous effect retards the momentum of buoyancy force and conductive heat transfer dominates the heat transfer mechanism.

At the highest computation of Rayleigh number in the present study, the central vortex points to the upper left and bottom right corners of the cavity indicating high fluid flow velocity drags the outer vortex. This can be seen as the velocity boundary layer becomes thinner near the differentially heated walls. The computed isotherms become parallel to the top and bottom walls indicates the convective heat transfer is the main heat transfer mechanism at this value of Rayleigh number. Denser isotherms near the walls indicate high value of local mean Nusselt number which contributes higher average Nusselt number in the system. All of the presented results are agree well with the previous studies[5][6][33].

Finally, Fig. 14 shows the comparison of streamlines and isotherms line for the computation at $Ra = 10^4$ and $\varepsilon = 0.6$. Excellent agreement can be seen when we superimposed the computed lines between the Navier-Stokes solution and the proposed approach.

4 Conclusion

The natural convection in a square cavity filled with porous medium has been simulated using the mesoscale numerical scheme where the Navier Stokes equation was solved indirectly using the

lattice Boltzmann method. The result of streamlines plots at three different porosity and three different Rayleigh numbers clearly depicting the flow pattern and vortex structure in the cavity. The central vortex is transformed from a circular to an elliptic shape when the Rayleigh number increases. The presence of porous medium contributes in decelerating the flow velocity in the system. Extension of work to three-dimensional formulation will be our next topic of research.

References:

- [1] D.V. Davis, Natural Convection of Air in a Square Cavity; A Benchmark Numerical Solution, *International Journal for Numerical Methods in Fluids*, Vol.3, No.3, 1983, pp. 249-264.
- [2] H.P.G. Darcy, *Les fontaines publiques de la ville de Dijon*, Victor Dalmont Paris, 1856.
- [3] H.C. Brinkman, A calculation of the viscous force exerted by a flowing fluid in a dense swarm of particles, *Applied Scientific Research*, Vol.1, No.1, 1949, pp. 27-34.
- [4] P. Forcheimer, Wasserbewegung durch Borden, *Zeitschrift des Verines Deutscher Ingenieure*, Vol.45, No.1, 1901, pp.1736-1741.
- [5] V. Prasad, Kulacki and M. Keyhani, Natural convection in porous media, *Journal of Fluid Mechanics*, Vol.150, No.1, 1985, pp.89-119.
- [6] P. Nithiarasu, K.N. Seetharamu and T. Sundarajan, Natural convective heat transfer in a fluid saturated variable porosity medium, *International Journal of Heat and Mass Transfer*, Vol.40, No.16, 1997, pp. 3955-3967
- [7] S. Chen and G.D. Doolen, Lattice Boltzmann method for fluid flows, *Annual Review Fluid Mechanics*, Vol.30, No.1, 1998, pp. 329-364.
- [8] X. He, S. Shan and G. Doolen, A Novel Thermal Model for Lattice Boltzmann Method in Incompressible Limit, *Journal of Computational Physics*, Vol.146, No.1, 1998, pp. 282-300.
- [9] C.S. Nor Azwadi and S. Syahrullail, A Three-Dimension Double-Population Thermal Lattice BGK Model for Simulation of Natural Convection Heat Transfer in a Cubic Cavity, *WSEAS Transaction on Mathematics*, Vol.8, No.9, 2009, pp. 561-571.
- [10] Y.H. Qian, D. Humieres and P. Lallemand, Lattice BGK for Navier-Stokes Equation, *Europhysics Letter*, Vol.17, No.6, 1992, pp. 479-484.
- [11] C.S.N. Azwadi and T. Tanahashi, Simplified thermal lattice Boltzmann in incompressible limit, *International Journal of Modern Physics B*. Vol.20, No.17, 2006, pp.2437-2449.
- [12] Y. Peng, C. Shu and Y.T. Chew, A 3D Incompressible Thermal Lattice Boltzmann Model and its Application to Simulation Natural Convection in a Cubic Cavity, *Journal of Computational Physics*, Vol.193, No.1, 2003, pp. 260-274.
- [13] X. He and L.S. Luo, Lattice Boltzmann Model for the Incompressible Navier-Stokes Equation, *Journal of Statistical Physics*, Vol.88, No.3, 1997, pp. 927-944.
- [14] G. Breyiannis and D. Valougeorgis, Lattice Kinetic Simulations in Three-Dimensional Magnetohydrodynamics, *Physical Review E*, Vol.69, No.6, 2004, pp. 065702/1-065702/4.
- [15] L. Jonas, B. Chopard, S. Succi and F. Toschi, Numerical Analysis of the Average Flow Field in a Turbulent Lattice Boltzmann Simulation, *Physica A*, Vol.362, No.1, 2006, pp. 6-10.
- [16] F. Nathan and H. Richard, Simulating Acoustic Propagation using a Lattice Boltzmann Model of Incompressible Fluid Flow, *WSEAS Transactions on Signal Processing*, Vol.2, No.6, 2006, pp. 876-881.
- [17] I. Halliday and C.M. Care, Steady State Hydrodynamics of Lattice Boltzmann Immiscible Lattice Gas, *Physical Review E*, Vol.53, No.2, 1996, pp. 1602-1612.
- [18] C.S. Michael and T.T. Daniel, *Lattice Boltzmann Modeling; An Introduction for Geoscientists and Engineers*, Springer, 2006.
- [19] S. Alapati, S. Kang and Y. K. Suh, 3D Lattice Boltzmann Simulation of Droplet Formation in a Cross-Junction Microchannel, *Proceeding of the 3rd IASME/WSEAS International Conference on Continuum Mechanics*, 2008.
- [20] C.S.N. Azwadi and N.C. Horng, Lattice Boltzmann Modelling of Microchannel Flow, *Journal of Materials Science and Engineering*, Vol.3, No. 12, 2009, pp. 17-21.
- [21] U. Frish, B. Hasslacher and Y. Pomeau, Lattice Gas Automata for the Navier-Stokes Equation, *Physical Review Letters*, Vol.56, No.14, 1986, pp. 1505-1508.
- [22] G. McNamara and B. Alder, Analysis of Lattice Boltzmann Treatment of Hydrodynamics, *Physica A*, Vol.194, No.1, 1993, pp. 218-228.
- [23] S. Hou, Q. Zou, S. Chen, G. Doolen and A. C. Cogley, Simulation of Cavity Flow by the Lattice Boltzmann Method, *Journal of Computational Physics*, Vol.118, No.2, 1995, pp. 329-347.

- [24] X. Shan and H. Chen, Lattice Boltzmann Model for Simulating Flows with Multiple Phases and Components, *Physical Review E*, Vol.47, No.3, 1993, pp. 1815-1820.
- [25] X. He and L.S. Luo, Lattice Boltzmann Model for the Incompressible Navier-Stokes Equation, *Journal of Statistical Physics*, Vol.88, No.3, 1997, pp. 927-944.
- [26] C.S. Nor Azwadi and T. Tanahashi, Simplified Finite Difference Thermal Lattice Boltzmann Method, *International Journal of Modern Physics B*, Vol.22, No.22, 2008, pp. 3865-3876.
- [27] H.N. Dixit and V. Babu, Simulation of High Rayleigh Number Natural Convection in a Square Cavity using the Lattice Boltzmann Method, *International Journal of Heat and Mass Transfer*, Vol.49, No.4, 2006, pp. 727-739.
- [28] P. Lallemand and L.S. Luo, Theory of the Lattice Boltzmann Method: Acoustic and Thermal Properties in Two and Three Dimensions, *Physical Review E*, Vol.68, No.3, 2003, pp. 036706/1-036706/25.
- [29] J. Onishi, Y. Chen and H. Ohashi, Lattice Boltzmann Simulation of Natural Convection in a Square Cavity, *JSME International Journal Series B*, Vol.44, No.1, 2001, pp. 45-52.
- [30] S. Harris, *An Introduction to the Theory of the Boltzmann Equation*, Holt, Rinehart and Winston, 1971.
- [31] P.L. Bhatnagar, E.P. Gross and M. Krook, A Model for Collision Process in Gasses. 1. Small Amplitude Processes in Charged and Neutral One-Component System, *Physical Review*, Vol.70, No.3, 1954, pp. 511-525.
- [32] C.S. Nor Azwadi and T. Tanahashi, Three Dimensional Thermal Lattice Boltzmann Simulation of Natural Convection in a Cubic Cavity, *International Journal of Modern Physics B*, Vol.21, No.1, 2007, pp. 87-96.
- [33] T. Seta, E. Takegoshi and K. Okui, Lattice Boltzmann simulation of natural convection in porous media, *Mathematics and Computers in Simulation*, Vol.72, No.1. 2006, pp.195-200.